Efficient Linearly and Unconditionally Energy Stable Schemes for the Phase Field Model of Solid-State Dewetting Problems

Zhengkang He[1], Jie Chen[1(✉)], and Zhangxin Chen[1,2]

[1] School of Mathematics and Statistics, Xi'an Jiaotong University, Shaanxi 710049, People's Republic of China
chenjiexjtu@mail.xjtu.edu.cn

[2] Schulich School of Engineering, University of Calgary, 2500 University Drive NW, Calgary, AB T2N 1N4, Canada

Abstract. In this paper, we study linearly first and second order in time, uniquely solvable and unconditionally energy stable numerical schemes to approximate the phase field model of solid-state dewetting problems based on the novel approach SAV (scalar auxiliary variable), a new developed efficient and accurate method for a large class of gradient flows. The schemes are based on the first order Euler method and the second order backward differential formulas(BDF2) for time discretization, and finite element methods for space discretization. It is shown that the schemes are unconditionally stable and the discrete equations are uniquely solvable for all time steps. We present some numerical experiments to validate the stability and accuracy of the proposed schemes.

Keywords: Phase field models · Solid-state dewetting · SAV
Energy stability · Surface diffusion · Finite element methods

1 Introduction

Solid-state dewetting of thin films plays an important role in many engineering and industrial applications, such as microelectronics processing, formation of patterned silicides in electronic devices, production of catalysts for the growth of carbon and semiconductor nanowires [2,4–6]. In general, solid-state dewetting can be modeled as interfacial dynamic problems where the morphological evolution is controlled by the surface diffusion. However, during the evolution, the interface may experience complicated topological changes such as pinch-off, splitting and fattening. All of them make great difficulties in the simulation of this interface evolution problem. The phase field model of solid-state dewetting problems presented in [1] can naturally capture topological changes that occur during the morphological evolution and can be easily extended to high dimension spaces. The idea of phase field approach dates back to the pioneering work

Y. Shi et al. (Eds.): ICCS 2018, LNCS 10862, pp. 102–112, 2018.
https://doi.org/10.1007/978-3-319-93713-7_8

of [12,16], which use an auxiliary variable ϕ (phase field function) to localize the phases and describe the interface by a layer of small thickness. Now, the phase field method becomes one of the major modeling and computational tools for the study of interfacial phenomena (cf. [3,7,10,11,17]), and the references therein).

From the numerical perspective, for phase field models, one main challenge in the numerical approximation is how to design unconditionally energy stable schemes which keep the energy dissipative in both semi-discrete and fully discrete forms. The preservation of the energy dissipation law is particularly important, and is critical to preclude the non-physical numerical solutions. In fact, it has been observed that numerical schemes which do not respect the energy dissipation law may lead to large numerical errors, particular for long time simulation, so it is specially desirable to design numerical schemes that preserve the energy dissipation law at the discrete level [7,8]. Another focus of developing numerical schemes to approximate the phase field models is to construct higher order time marching schemes. Under the requests of some degree of accuracy, higher order time marching schemes are usually preferable to lower order time marching schemes when we want to use larger time marching steps to achieve long time simulation [9–11]. This fact motivates us to develop more accurate schemes. Moreover, it goes without saying that linear numerical schemes are more efficient than the nonlinear numerical schemes because the nonlinear scheme are expensive to solve.

In this paper, we study linearly first and second order accurate in time, uniquely solvable and unconditionally energy stable numerical schemes for solving the phase field model of solid-state dewetting problems based on the SAV (scalar auxiliary variable) approach which are applicable to a large class of gradient flows [13,14]. The essential idea of the SAV approach is to split the total free energy $\mathcal{E}(\phi)$ of gradient flows into two parts, written as

$$\mathcal{E}(\phi) = \frac{1}{2}(\phi, \mathcal{L}\phi) + \mathcal{E}_1(\phi), \tag{1}$$

where $\mathcal{L}$ is a symmetric non-negative linear operator contains the highest linear derivative terms in $\mathcal{E}$, and $\mathcal{E}_1(\phi) \geq C > 0$ is the nonlinear term but with only lower order derivative than $\mathcal{L}$. Then the SAV approach transform the nonlinear term $\mathcal{E}_1$ into quadratic form by only introduce a scalar variable $r = \sqrt{\mathcal{E}_1}$ and the total free energy $\mathcal{E}$ can be written as

$$\mathcal{E}(\phi, r) = \frac{1}{2}(\phi, \mathcal{L}\phi) + r^2. \tag{2}$$

The rest of the paper is organized as follows. In Sect. 2, we describe the phase field model of solid-state dewetting problems and the associated energy law. In Sect. 3, we develop linear numerical schemes with first order and second order accuracy in time for simulating the model, and prove their unconditional energy stabilities and unconditionally unique solvability. In Sect. 4, some numerical experiments are performed to validate the accuracy and energy stability of the proposed schemes. Finally, some concluding remarks are given in Sect. 5.

2 The Governing System and Energy Law

We now give a brief introduction to the phase field model as is proposed in [1] that simulates the solid-state dewetting phenomenon of thin films and the morphological evolution of patterned islands on a solid substrate. If we consider that the free interface (surface between thin film phase and vapor phase) energy is isotropic, then the total free energy of the system is defined as follows

$$\mathcal{E}(\phi) = \mathcal{E}_{FV}(\phi) + \mathcal{E}_w(\phi) = \int_\Omega f_{FV}(\phi)\mathrm{d}\mathbf{x} + \int_{\Gamma_w} f_w(\phi)\mathrm{d}s \tag{3}$$

here Ω is a bounded domain in $\mathbb{R}^2$, with boundary $\partial\Omega$ that has an outward-pointing unit normal $\mathbf{n}$. $\Gamma_w \subseteq \partial\Omega$ represents the solid surface (solid substrate) to where the thin film adhere, called as wall boundary. $\mathcal{E}_{FV}$ represents the free interface energy of two phases (thin film phase and vapor phase), $\mathcal{E}_w$ represents the combined energy on the solid surface called wall energy, and f_{FV} and f_w are the corresponding energy densities, respectively, defined as follows

$$f_{FV}(\phi) = F(\phi) + \frac{\varepsilon^2}{2}|\nabla\phi|^2 \tag{4}$$

$$f_w(\phi) = \frac{\varepsilon(\phi^3 - 3\phi)}{3\sqrt{2}}\cos\theta_s. \tag{5}$$

where $F(\phi) = \frac{1}{4}(\phi^2-1)^2$ is the well-known Ginzburg-Landau double-well potential, ε is a positive constant related to the interface width, and θ_s is the prescribed contact angle between the free interface and the solid surface.

The governing equations of the system is defined as follows

$$\frac{\partial\phi}{\partial t} = \nabla\cdot(M(\phi)\nabla\mu), \qquad \text{in } \Omega \tag{6}$$

$$\mu = \frac{\delta\mathcal{E}}{\delta\phi} = \phi^3 - \phi - \varepsilon^2\Delta\phi, \qquad \text{in } \Omega \tag{7}$$

with the following boundary conditions

$$\varepsilon^2\frac{\partial\phi}{\partial\mathbf{n}} + f_w' = 0, \quad \frac{\partial\mu}{\partial\mathbf{n}} = 0, \qquad \text{on } \Gamma_w \tag{8}$$

$$\frac{\partial\phi}{\partial\mathbf{n}} = 0, \quad \frac{\partial\mu}{\partial\mathbf{n}} = 0, \qquad \text{on } \partial\Omega\backslash\Gamma_w \tag{9}$$

The above system can be derived as a gradient flow of the total free energy functional $\mathcal{E}(\phi)$ with the dissipation mechanism $\nabla\cdot(M(\phi)\nabla\mu)$, where $M(\phi) = 1-\phi^2$ is the mobility function chosen in [1] and μ is the first variational derivative of the total free energy $\mathcal{E}$ with respect to the phase field variable ϕ called the chemical potential. The boundary condition $\frac{\partial\mu}{\partial\mathbf{n}} = 0$ implies that the total mass is conservative:

$$\frac{d}{dt}\int_\Omega \phi\mathrm{d}\mathbf{x} = \int_\Omega \phi_t\mathrm{d}\mathbf{x} = \int_\Omega \nabla\cdot(M(\phi)\nabla\mu)\mathrm{d}\mathbf{x} = -\int_\Omega M(\phi)\frac{\partial\mu}{\partial\mathbf{n}}\mathrm{d}s = 0. \tag{10}$$

Moreover, the total free energy functional $\mathcal{E}(t)$ is dissipative:

$$\begin{aligned}\frac{d}{dt}\mathcal{E}(t) &= \int_\Omega F^{'}(\phi)\phi_t + \varepsilon^2\nabla\phi\cdot\nabla\phi_t \mathrm{d}\mathbf{x} + \int_{\Gamma_w} f_w^{'}(\phi)\phi_t \mathrm{d}s \\ &= \int_\Omega \mu\phi_t \mathrm{d}\mathbf{x} + \int_{\Gamma_w}\big(\varepsilon^2\frac{\partial\phi}{\partial\mathbf{n}} + f_w^{'}(\phi)\big)\phi_t \mathrm{d}s = \int_\Omega \mu M\triangle\mu \mathrm{d}\mathbf{x} \\ &= -\int_\Omega M\nabla\mu\cdot\nabla\mu \mathrm{d}\mathbf{x} + \int_{\partial\Omega}\mu M\frac{\partial\mu}{\partial\mathbf{n}}\mathrm{d}s \\ &= -\int_\Omega M|\nabla\mu|^2\mathrm{d}\mathbf{x} \le 0 \end{aligned} \tag{11}$$

3 Numerical Schemes and Energy Stability

In this section, we construct several fully discrete numerical schemes for solving the dewetting problems, and prove their energy stabilities and unique solvability.

We aim to obtain some effective numerical schemes, in particular, the linear schemes. Inspired by the SAV approach, we split the total free energy $\mathcal{E}$ as follows,

$$\begin{aligned}\mathcal{E}(\phi) &= \frac{\varepsilon^2}{2}(\nabla\phi,\nabla\phi) + \frac{1}{4}\int_\Omega(\phi^2-1)^2\mathrm{d}\mathbf{x} + \int_{\Gamma_w}\frac{\phi^3-3\phi}{3\sqrt{2}}\varepsilon\cos\theta_s\mathrm{d}s \\ &= \frac{\varepsilon^2}{2}(-\Delta\phi,\phi) + \frac{\varepsilon^2}{2}\int_{\partial\Omega}\frac{\partial\phi}{\partial\mathbf{n}}\phi\mathrm{d}s + \frac{\beta}{2}\int_\Omega\phi^2\mathrm{d}\mathbf{x} + \frac{1}{4}\int_\Omega(\phi^2-1-\beta)^2\mathrm{d}\mathbf{x} \\ &\quad + \int_{\Gamma_w}\frac{\phi^3-3\phi}{3\sqrt{2}}\varepsilon\cos\theta_s\mathrm{d}s - \frac{1}{4}\int_\Omega\beta^2+2\beta\mathrm{d}\mathbf{x} \\ &= \frac{1}{2}(\phi,\mathcal{L}\phi) + \mathcal{E}_1(\phi) - \frac{1}{4}\int_\Omega\beta^2+2\beta\mathrm{d}\mathbf{x} \end{aligned} \tag{12}$$

where β is a positive constant to be chosen, and

$$\begin{aligned}(\phi,\mathcal{L}\phi) &= \varepsilon^2(-\Delta\phi,\phi) + \varepsilon^2\int_{\partial\Omega}\frac{\partial\phi}{\partial\mathbf{n}}\phi\mathrm{d}s + \beta\int_\Omega\phi^2\mathrm{d}\mathbf{x} = \varepsilon^2(\nabla\phi,\nabla\phi) + \beta(\phi,\phi) \\ \mathcal{E}_1(\phi) &= \frac{1}{4}\int_\Omega(\phi^2-1-\beta)^2\mathrm{d}\mathbf{x} + \int_{\Gamma_w}\frac{\phi^3-3\phi}{3\sqrt{2}}\varepsilon\cos\theta_s\mathrm{d}s. \end{aligned}$$

We drop the constant $-\frac{1}{4}\int_\Omega\beta^2+2\beta\mathrm{d}x$ in the total free energy $\mathcal{E}(\phi)$, then the total free energy becomes as

$$\mathcal{E}(\phi) = \frac{1}{2}(\phi,\mathcal{L}\phi) + \mathcal{E}_1(\phi), \tag{13}$$

and the gradient flow Eqs. (6) and (7) can be written as

$$\frac{\partial\phi}{\partial t} = \nabla\cdot((1-\phi^2)\nabla\mu), \tag{14}$$

$$\mu = \mathcal{L}\phi + U(\phi), \tag{15}$$

where,

$$U(\phi) = \frac{\delta \mathcal{E}_1}{\delta \phi} \tag{16}$$

is the first variational derivative of the free energy $\mathcal{E}_1$ with respect to the phase field variable ϕ.

As in [13,14], a scalar auxiliary variable $r = \sqrt{\mathcal{E}_1}$ is introduced, then we rebuild the total free energy functional (12) as

$$\mathcal{E}(\phi, r) = \frac{1}{2}(\phi, \mathcal{L}\phi) + r^2, \tag{17}$$

and accordingly we can rewrite the gradient flow Eqs. (14) and (15) as follows

$$\frac{\partial \phi}{\partial t} = \nabla \cdot ((1 - \phi^2)\nabla \mu), \tag{18}$$

$$\mu = \mathcal{L}\phi + \frac{r}{\sqrt{\mathcal{E}_1(\phi)}} U(\phi), \tag{19}$$

$$r_t = \frac{1}{2\sqrt{\mathcal{E}_1(\phi)}} \langle U(\phi), \phi_t \rangle. \tag{20}$$

where,

$$\langle U(\phi), \psi_t \rangle = \int_\Omega (\phi^3 - \phi - \beta\phi)\psi_t \mathrm{d}\mathbf{x} + \int_{\Gamma_w} \frac{\sqrt{2}}{2}(\phi^2 - 1)\varepsilon \cos\theta_s \psi_t \mathrm{d}s. \tag{21}$$

The boundary conditions are also (8) and (9), and the initial conditions are

$$\phi(x, y, 0) = \phi_0, r(0) = \sqrt{\mathcal{E}_1(\phi_0)} \tag{22}$$

Taking the inner products of the Eqs. (18)–(20) with μ, $\frac{\partial \phi}{\partial t}$ and $2r$ respectively, the new system still follows an energy dissipative law:

$$\frac{d}{dt}\mathcal{E}(\phi, r) = \frac{d}{dt}[(\phi, \mathcal{L}\phi) + r^2] = -(\mu, M(\phi)\mu) \leq 0. \tag{23}$$

Remark: β is a positive number to be chosen.

Since finite element methods have the capability of handling complex geometries, we consider the fully discrete numerical schemes for solving the system (18)–(20) in the framework of finite element methods. Let $\mathcal{T}_h$ be a quasi-uniform triangulation of the domain Ω of mesh size h. We introduce the finite element space S_h to approximate the Sobolev space $H^1(\Omega)$ based on the triangulation $\mathcal{T}_h$.

$$S_h = \{v_h \in C(\Omega) \mid v_h| \in P_r, \forall \in \mathcal{T}_h\}, \tag{24}$$

where P_r is the space of polynomials of degree at most r. Denote the time step by δt and set $t^n = n\delta t$. Firstly, we give the fully discrete scheme of first order.

3.1 The Fully Discrete Linear First Order Scheme

In the framework of finite element space above, we now give the fully discrete semi-implicit first order scheme for the system (18)–(20) based on the backward Euler's method. Assuming that ϕ_h^n and r_h^n are already known, we find $(\phi_h^{n+1}, \mu_h^{n+1}, r_h^{n+1}) \in S_h \times S_h \times \mathbb{R}^+$ such that for all $(\nu_h, \psi_h) \in S_h \times S_h$ there hold

$$\Big(\frac{\phi_h^{n+1}-\phi_h^n}{dt}, \nu_h\Big) = -\big(\,|1-(\phi_h^n)^2|\,\nabla\mu_h^{n+1}, \nabla\nu_h\big), \tag{25}$$

$$\big(\mu_h^{n+1}, \psi_h\big) = \big(\mathcal{L}\phi_h^{n+1}, \psi_h\big) + \frac{r_h^{n+1}}{\sqrt{\mathcal{E}_1(\phi_h^{n+1})}}\langle U(\phi_h^n), \psi_h\rangle, \tag{26}$$

$$r_h^{n+1} - r_h^n = \frac{1}{2\sqrt{\mathcal{E}_1(\phi_h^n)}}\langle U(\phi_h^n), \phi_h^{n+1}-\phi_h^n\rangle. \tag{27}$$

where

$$\begin{aligned}(\mathcal{L}\phi_h^{n+1}, \psi_h) &= \varepsilon^2(-\Delta\phi_h^{n+1}, \psi) + \varepsilon^2\int_{\partial\Omega}\frac{\partial\phi_h^{n+1}}{\partial\mathbf{n}}\psi_h \mathrm{d}s + \beta\int_\Omega \phi_h^{n+1}\psi_h \mathrm{d}\mathbf{x}\\ &= \varepsilon^2(\nabla\phi_h^{n+1}, \nabla\psi_h) + \beta(\phi_h^{n+1}, \psi_h)\end{aligned} \tag{28}$$

and

$$\begin{aligned}\langle U[\phi_h^{n+1}], \psi_h\rangle = &\int_\Omega \big((\phi_h^{n+1})^3 - \phi_h^{n+1} - \beta\phi_h^{n+1}\big)\psi_h \mathrm{d}\mathbf{x}\\ &+ \int_{\Gamma_w}\frac{\sqrt{2}}{2}\big((\phi_h^{n+1})^2 - 1\big)\varepsilon\cos\theta_s\psi_h \mathrm{d}s.\end{aligned} \tag{29}$$

Remark: Taking $\nu_h = 1$ in Eq. (25), we obtain the conservation of the total mass,

$$\int_\Omega \phi_h^{n+1}\mathrm{d}\mathbf{x} = \int_\Omega \phi_h^n \mathrm{d}\mathbf{x} = \cdots = \int_\Omega \phi_h^0 \mathrm{d}\mathbf{x} \tag{30}$$

Theorem 1. *Given $(\phi_h^n, r_h^n) \in S_h \times \mathbb{R}^+$, the system (25)–(27) admits a unique solution $(\phi_h^{n+1}, \mu_h^{n+1}, r_h^{n+1}) \in S_h \times S_h \times \mathbb{R}^+$ at the time t^{n+1} for any $h > 0$ and $\delta t > 0$. Moreover, the solution satisfies a discrete energy law as follows*

$$\begin{aligned}\mathcal{E}_{1st}^{n+1} - \mathcal{E}_{1st}^n + \frac{1}{2}(\phi_h^{n+1}-\phi_h^n, \mathcal{L}(\phi_h^{n+1}-\phi_h^n)) + (r_h^{n+1}-r_h^n)^2\\ = -\delta t(\big|1-(\phi_h^n)^2\big|\,\nabla\mu_h^{n+1}, \nabla\mu_h^{n+1})\end{aligned}$$

where $\mathcal{E}_{1st}^{n+1}$ is the modified energy

$$\mathcal{E}_{1st}^n = \frac{1}{2}(\phi_h^n, \mathcal{L}\phi_h^n) + (r_h^n)^2. \tag{31}$$

Thus the scheme is unconditionally stable.

Proof. Taking $\nu_h = \mu^{n+1}$ and $\psi_h = (\phi^{n+1}-\phi^n)/\delta t$ in Eqs. (25) and (26) respectively and adding Eqs. (25)–(27) together, we can obtain the discrete energy law, in addition, the schemes (25)–(27) is a linear system, thus there exists a unique solution $(\phi_h^{n+1}, \mu_h^{n+1}, r_h^{n+1})$ at time t^{n+1}.

3.2 The Fully Discrete Linear Second Order Scheme

We now give the fully discrete semi-implicit second order scheme for the system (18)–(20) based on the backward differentiation formula (BDF2). Assuming that ϕ_h^{n-1}, r_h^{n-1}, ϕ_h^n and r_h^n are already known, we find $(\phi_h^{n+1}, \mu_h^{n+1}, r_h^{n+1}) \in S_h \times S_h \times \mathbb{R}^+$ such that for all $(\nu_h, \psi_h) \in S_h \times S_h$ there hold

$$\left(\frac{3\phi_h^{n+1} - 4\phi_h^n + \phi_h^{n-1}}{2\delta t}, \nu_h\right) = -\left(\left|1 - (\bar{\phi}_h^{n+1})^2\right| \nabla\mu_h^{n+1}, \nabla\nu_h\right) \tag{32}$$

$$\left(\mu_h^{n+1}, \psi_h\right) = \left(\mathcal{L}\phi_h^{n+1}, \psi_h\right) + \frac{r_h^{n+1}}{\sqrt{\mathcal{E}_1(\bar{\phi_h}^{n+1})}}\langle U(\bar{\phi}_h^{n+1}), \psi_h\rangle, \tag{33}$$

$$3r_h^{n+1} - 4r_h^n + r_h^{n-1} = \frac{1}{2\sqrt{\mathcal{E}_1(\bar{\phi}_h^{n+1})}}\langle U(\bar{\phi}_h^{n+1}), 3\phi_h^{n+1} - 4\phi_h^n + \phi_h^{n-1}\rangle, \tag{34}$$

where $\bar{\phi}_h^{n+1} = 2\phi_h^n - \phi_h^{n-1}$,

$$\begin{aligned}(\mathcal{L}\phi_h^{n+1}, \psi_h) &= \varepsilon^2(-\Delta\phi_h^{n+1}, \psi) + \varepsilon^2\int_{\partial\Omega}\frac{\partial\phi_h^{n+1}}{\partial\mathbf{n}}\psi_h \mathrm{d}s + \beta\int_\Omega \phi_h^{n+1}\psi_h \mathrm{d}\mathbf{x}\\ &= \varepsilon^2(\nabla\phi_h^{n+1}, \nabla\psi_h) + \beta(\phi_h^{n+1}, \psi_h),\end{aligned} \tag{35}$$

and

$$\begin{aligned}\langle U[\bar{\phi}_h^{n+1}], \psi_h\rangle = &\int_\Omega \left((\bar{\phi}_h^{n+1})^3 - \bar{\phi}_h^{n+1} - \beta\bar{\phi}_h^{n+1}\right)\psi_h \mathrm{d}\mathbf{x}\\ &+ \int_{\Gamma_w}\frac{\sqrt{2}}{2}\left((\bar{\phi}_h^{n+1})^2 - 1\right)\varepsilon\cos\theta_s\psi_h \mathrm{d}s.\end{aligned} \tag{36}$$

Remark: The second order scheme (32)–(34) is a two step method, we can solve for ϕ_h^1 and r_h^1 through the first order scheme (25)–(27), similarly by taking $\nu_h = 1$ in Eq. (32), we obtain the conservation of the total mass,

$$\int_\Omega \phi_h^{n+1}\mathrm{d}\mathbf{x} = \int_\Omega \phi_h^n \mathrm{d}\mathbf{x} = \cdots = \int_\Omega \phi_h^0 \mathrm{d}\mathbf{x} \tag{37}$$

Theorem 2. *Given $(\phi_h^n, r_h^n) \in S_h \times \mathbb{R}^+$, the system (32)–(34) admits a unique solution $(\phi_h^{n+1}, \mu_h^{n+1}, r_h^{n+1}) \in S_h \times S_h \times \mathbb{R}^+$ at the time t^{n+1} for any $h > 0$ and $\delta t > 0$. Moreover, the solution satisfies a discrete energy law as follows*

$$\begin{aligned}&\mathcal{E}_{2nd}^{n+1,n} - \mathcal{E}_{2nd}^{n,n-1} + \frac{1}{4}\left(\phi_h^{n+1} - 2\phi_h^n + \phi_h^{n-1}, \mathcal{L}(\phi_h^{n+1} - 2\phi_h^n + \phi_h^{n-1})\right)\\ &\quad + \frac{1}{2}(r_h^{n+1} - 2r_h^n + r_h^{n-1})^2 = -\delta t\left(\left|1 - (\bar{\phi}_h^{n+1})^2\right| \nabla\mu_h^{n+1}, \nabla\mu_h^{n+1}\right)\end{aligned}$$

where $\mathcal{E}_{2nd}^{n+1,n}$ is the modified energy

$$\mathcal{E}_{2nd}^{n+1,n} = \frac{1}{4}\left(\left(\phi_h^{n+1}, \mathcal{L}\phi_h^{n+1}\right) + \left(2\phi_h^{n+1} - \phi_h^n, \mathcal{L}(2\phi_h^{n+1} - \phi_h^n)\right) + \frac{1}{2}\left((r_h^{n+1})^2 + (2r_h^{n+1} - r_h^n)^2\right)\right) \tag{38}$$

Proof. Taking $\nu_h = \mu_h^{n+1}$ and $\psi_h = (3\phi_h^{n+1} - 4\phi_h^n + \phi_h^{n-1})/\delta t$ in Eqs. (32) and (33) respectively integrating the first two equations and applying the following identity:

$$2(3a^{k+1} - 4a^k + a^{k-1}, a^{k+1}) = \left|a^{k+1}\right|^2 + \left|2a^{k+1} - a^k\right|^2 + \left|a^{k+1} - 2a^k + a^{k-1}\right|^2 - \left|a^k\right|^2 - \left|2a^k - a^{k-1}\right|^2, \tag{39}$$

we can obtain the discrete energy law, in addition, the schemes (32)–(34) is a linear system, thus there exists a unique solution $(\phi_h^{n+1}, \mu_h^{n+1}, r_h^{n+1})$ at time t^{n+1}.

4 Numerical Experiments

In this section, we present some numerical experiments to validate the accuracy and stability of numerical schemes presented in this paper. For simplicity, we use the conforming P_1 finite element in space S_h to approximate ϕ_h and μ_h. For all our experiments in this section, the computational domain is taken as a rectangle $\Omega = [-1, 1] \times [0, 1]$, and the wall boundary Γ_w is the bottom of the rectangle domain, defined as

$$\Gamma_w = \{(x, y) | -1 < x < 1, y = 0\}.$$

The algorithms are implemented in MATLAB using the software library *i*FEM [15].

4.1 Convergence Test

In this subsection, we provide some numerical evidence to show the second order temporal accuracy for the numerical scheme (32)–(34) by the method of Cauchy convergence test as in [17]. We consider the problem with an given initial condition but with no explicit exact solution. The domain Ω is triangulated by a structured mesh with uniform 2^{k+1} grid points in the x direction and uniform 2^k grid points in the y direction, for k from 4 to 8. The final time is taken to be $T = 0.1$ and the time step is taken to be $\delta t = 0.2h$. Since the P_1 finite element approximation is used for the phase field variable ϕ_h, the L^2 norm of the Cauchy difference error $\|\phi_h^k - \phi_h^{k-1}\|$ is expected to converge to zero at the rate of second order $err = O(\delta t^2) + O(h^2) = O(\delta t^2)$. The initial condition of the phase field variable ϕ is taken to be

$$\phi_0(x, y) = \tanh\left(\frac{0.25 - \sqrt{x^2 + y^2}}{\sqrt{2}\varepsilon}\right), \tag{40}$$

We take parameters $\varepsilon = 0.1$, $\beta = 5$ and use five different contact angles $\theta_s = \pi$, $\theta_s = 3\pi/4$, $\theta_s = \pi/2$, $\theta_s = \pi/4$, $\theta_s = 0$ to test the convergence rate respectively, The Cauchy errors and the relative convergence rates are presented in Table 1 which shows the second order convergence for all cases.

Table 1. Cauchy convergence test for the second order linear numerical scheme (32)–(34) with the initial condition (40), parameters are $\varepsilon = 0.1$ and $\beta = 5$, errors are measured in L^2 norm; 2^{k+1} and 2^k grid points in the x and y direction for k from 4 to 8, five different contact angles $\theta_s = \pi$, $\theta_s = 3\pi/4$, $\theta_s = \pi/2$, $\theta_s = \pi/4$, $\theta_s = 0$ are tested respectively

θ	$16-32$	Cvg. rate	$32-64$	Cvg. rate	$64-128$	Cvg. rate	$128-256$
π	0.0063	1.9480	0.0016	2.0777	3.8837e-004	2.1738	8.9332e-005
$3\pi/4$	0.0063	1.9505	0.0016	2.0246	3.9578e-004	2.0869	9.4824e-005
$\pi/2$	0.0061	1.9379	0.0016	1.9797	3.9895e-004	1.9978	9.9849e-005
$\pi/4$	0.0066	1.9218	0.0017	1.9882	4.2918e-004	2.0253	1.0596e-004
0	0.0069	1.9084	0.0018	1.9850	4.5246e-004	2.0179	1.1211e-004

4.2 Solid-State Dewetting Simulation in Two Dimension

In this subsection, we present some two-dimensional simulations for the solid-state dewetting problems using the schemes (32)–(34). The initial state of the thin film is taken to be a small rectangle:

$$\phi_0(x,y) = \begin{cases} 1 & \text{if} -0.5 \le x \le 0.5 \,\text{and}\, 0 \le y \le 0.2 \\ -1 & \text{otherwise.} \end{cases} \tag{41}$$

the computational parameters are taken as $\varepsilon = 0.01$ and $\delta t = 1/128$. Numerical simulations in [18] suggest that in order to accurately capture the interfacial dynamics, at least 4 elements are needed across the interfacial region of thickness

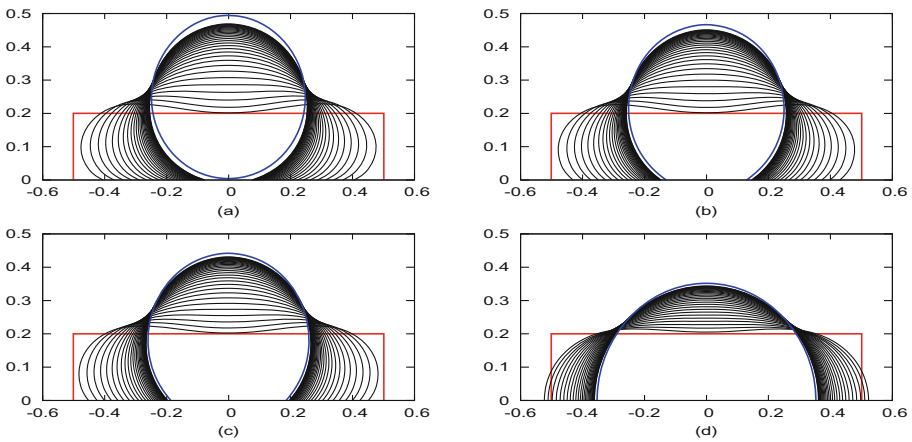

Fig. 1. The evolution of thin film for four different prescribed contact angles: (a) $\theta_s = \pi$, (b) $\theta_s = 5\pi/6$, (c) $\theta_s = 3\pi/4$, (d) $\theta_s = \pi/2$. The film profiles are shown every 2500 time steps (labeled as black lines). The red line and blue line represent the initial and numerical equilibrium states, respectively. (Color figure online)

$\sqrt{2}\varepsilon$. We explore adaptive mesh refinement algorithm of the software library iFEM [15] with the finest element size $h = 1/256$ to improve the computational efficiency. We examine the evolution of thin film under 4 different prescribed contact angles: $\theta_s = \pi$, $\theta_s = 5\pi/6$, $\theta_s = 3\pi/4$, $\theta_s = \pi/2$, respectively. The results are shown in Fig. 1.

We plot dissipative curve of the modified free energy in Fig. 2. Using five different time step of $\delta t = 0.01, 0.05, 0.1, 0.5, 1$ with the prescribed contact angle $\theta_s = \pi/2$. We observe that the energy decreases at all times, which confirms that our algorithm is unconditionally stable, as predicted by the theory.

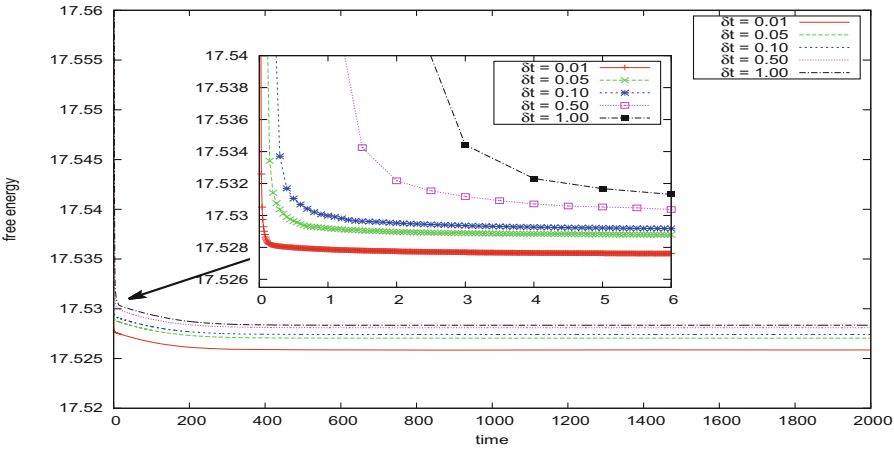

Fig. 2. Time evolution of the free energy functional for five different time steps of $\delta t = 0.01, 0.05, 0.1, 0.5, 1$ with the prescribed contact angle $\theta_s = \pi/2$. The energy curves show the decays for all time steps, which confirms that our algorithm is unconditionally stable.

5 Conclusions

In this paper, we present linearly first and second order in time, uniquely solvable and unconditionally energy stable schemes for solving the solid-state dewetting problems based on the novel SAV approach. We verify numerically that our schemes are up to second order accurate in time. Adaptive strategy is used to improve the efficiency of the algorithm. Numerical examples are presented to illustrate the stability and accuracy of the proposed schemes.

References

1. Jiang, W., Bao, W.: Phase field approach for simulating solid-state dewetting problems. Acta Mater. **60**, 5578–5592 (2012)
2. Mordehai, D., Kazakevich, M.: Nanoindentation size effect in single-crystal nanoparticles and thin films: a comparative experimental and simulation study. Acta Mater. **59**, 2309–2321 (2011)
3. Chen, J., Sun, S., Wang, X.: A numericalmethod for a model of two-phase flow in a coupled free flow and porous media system. J. Comput. Phys. **268**, 1–16 (2014)
4. Jiang, W., Wang, Y.: Solid-state dewetting and island morphologies in strongly anisotropic materials. Scripta Mater. **115**, 123–127 (2016)
5. Jiran, E., Thompson, C.V.: Capillary instabilities in thin films. J. Electron. Mater. **19**, 1153–1160 (1990)
6. Jiran, E., Thompson, C.V.: Capillary instabilities in thin, continuous films. Thin Solid Films **208**, 23–28 (1992)
7. Lee, H.G., Kim, J.: Accurate contact angle boundary conditions for the Cahn-Hilliard equations. Comput. Fluids **44**, 178–186 (2011)
8. Guillengonzalez, F., Tierra, G.: On linear schemes for a Cahn-Hilliard diffuse interface model. J. Comput. Phys. **234**, 140–171 (2013)
9. Han, D., Brylev, A.: Numerical analysis of second order, fully discrete energy stable schemes for phase field models of two-phase incompressible flows. J. Sci. Comput. **70**, 965–989 (2017)
10. Yang, X., Ju, L.: Efficient linear schemes with unconditional energy stability for the phase field elastic bending energy model. Comput. Methods Appl. Mech. Eng. **315**, 691–712 (2017)
11. Yang, X., Han, D.: Linearly first- and second-order, unconditionally energy stable schemes for the phase field crytal model. J. Comput. Phys. **330**, 1116–1134 (2017)
12. Rayleigh, L.: On the theory of surface forces. II. Compressible fluids. Philos. Mag. Ser. 1 **33**(201), 209–220 (1892)
13. Shen, J., Xu, J.: The scalar auxiliary variable (SAV) approach for gradient flows. J. Comput. Phys. **353**, 407–416 (2017)
14. Shen, J., Xu, J.: A new class of efficient and robust energy stable schemes for gradient flows. SIAM Reviews (to appear)
15. Chen, L.: An integrated finite element methods package in matlab, technical report, University of California at Irvine (2009)
16. Der Waals, J.D.: The thermodynamic theory of capillarity under the hypothesis of a continuous variation of density. J. Stat. Phys. **20**(2), 200–244 (1979)
17. Han, D., Wang, X.: A second order in time, uniquely solvable, unconditionally stable numerical scheme for Cahn-Hilliard-Navier-Stokes equation. J. Comput. Phys. **290**, 139–156 (2015)
18. Kim, J., Kang, K.: Conservative multigrid methods for Cahn-Hilliard fluids. J. Comput. Phys. **193**, 511–543 (2004)